Experimental and Numerical Analysis of Strain Rate Dependent Mechanical Behaviour of Fused Deposition Modelling (FDM) Printed Parts

Zulqarnain Mukhtar Mahmood[1], Hamza Malik[2], Zeeshan Khursheed[2], Muhammad Asif[2], Syed Asad Ali Zaidi[3,*]

[1] Department of Industrial Engineering, University of Naples Federico II, Napoli, Italy

[2] Department of Engineering Science, Pakistan Navy Engineering College, National University of Sciences and Technology, Karachi, Pakistan

[3] Department of Mechanical Engineering, Faculty of Engineering, Islamic University of Madinah, Medina 42351, Saudi Arabia

*Correspondence: Sali@iu.edu.sa

Abstract

Fused deposition modeling (FDM) of polylactic acid (PLA) is increasingly used for load-bearing components in consumer, biomedical, and engineering devices, yet its strain-rate-dependent mechanical performance is not fully quantified. This study aims to characterize quasi-static strain-rate sensitivity of FDM-printed PLA and to identify how build orientation, raster angle, and infill pattern can be tuned to improve tensile behavior. ASTM D638 Type-V dog-bone specimens were fabricated on Ender 3 Pro and Xplorer 3D printers and tested in tension at three benchmark crosshead speeds (2, 5, and 10 mm/s) representing quasi-static service conditions. Additional benchmark series investigated three build orientations (0°, 90°, and on-edge), three raster angles (0°, 15°, and 45°), and two infill patterns (concentric and hexagonal). Tensile strength increased by up to 115% when crosshead speed was raised from 2 to 10 mm/s,

while failure strain decreased, indicating more brittle behavior at higher rates. On-edge and 0°-oriented specimens reached maximum strengths of 32.3 MPa, 0° raster angles aligned with loading axis provided largest load-bearing capacity, and concentric infill outperformed hexagonal infill (26.4 vs 20.2 MPa). Finite element simulations performed in Ansys and Abaqus reproduced measured stress–strain curves and failure trends within a few megapascals. The combined experimental–numerical results show that careful selection of strain rate, orientation, and infill strategy is essential when designing FDM-printed PLA components for structurally reliable engineering and biomedical applications.

Keywords: Polylactic Acid (PLA), Fused Deposition Modelling (FDM), Strain-Rate Dependency, Build Orientation, Mechanical Properties, Numerical Modelling

1. Introduction

Polylactic acid (PLA) is a biodegradable thermoplastic polymer derived from renewable resources such as corn starch or sugarcane, making it an environmentally friendly alternative to conventional petroleum-based polymers [1] , [2]. With mechanical properties comparable to widely used polymers like polyethylene (PE) and polyethylene terephthalate (PETE), PLA offers additional advantages such as compost ability and low environmental impact. These features have expanded the use of PLA beyond packaging and into biomedical, agricultural, construction, electronics, and transportation applications [2] ; however, many of these more demanding uses rely on PLA blends or fiber-reinforced PLA composites, whereas neat PLA is mainly employed in packaging, disposable items, and low-to-moderate load structural components [2-4].

In biomedical contexts, PLA is commonly employed in internal implants, including interference screws, fixation tacks, and resorbable plates for orthopedic repairs [5]. Its

biocompatibility and degradability have also made it suitable for drug delivery systems and surgical sutures [6, 7]. Chemically, PLA belongs to the aliphatic polyester family and is synthesized from lactic acid (2-hydroxypropionic acid). Its properties—such as low processing temperature, tunable barrier characteristics, optical clarity, and the ability to form complex geometries—make it well-suited for advanced manufacturing, particularly fused deposition modeling (FDM) [8].

Despite these advantages, neat PLA also exhibits several important mechanical limitations. It is a relatively brittle polymer, with typical elongation at break values below 5%, and shows limited impact resistance compared with engineering thermoplastics such as ABS. In addition, its heat deflection temperature is close to its glass-transition temperature (≈55–65 °C), so the stiffness and strength of PLA parts can deteriorate rapidly under moderately elevated temperatures or sustained loads. These characteristics are critical when evaluating the performance of FDM-printed PLA components under mechanical loading and motivate a more detailed investigation of their strain-rate-dependent tensile behavior.

Additionally, PLA is known for its excellent printability and environmental biodegradability, which make it attractive for both industrial and consumer applications. The polymer was originally introduced by Carothers in 1932, though its early properties were considered unsatisfactory for widespread application [9]. Continued material enhancements led to the development of high-strength PLA, which was approved for clinical resorbable dressing applications in 1954 and later in 1972 [10] . A significant commercial milestone occurred in 1997 when Cargill Dow LLC and Purac Biochem B.V. announced a joint venture to bring PLA to the market [11]. Since then, PLA-based products have been commercialized in various forms and continue to gain traction. In additive manufacturing, particularly FDM, process parameters such as raster angle, layer height,

infill density, and build orientation critically influence the final part properties. These parameters can lead to anisotropic behavior, where properties differ along different directions of the printed part. See **Figure 1**. Time-dependent deformation, influenced by strain rate, also plays a role in performance under mechanical loads.

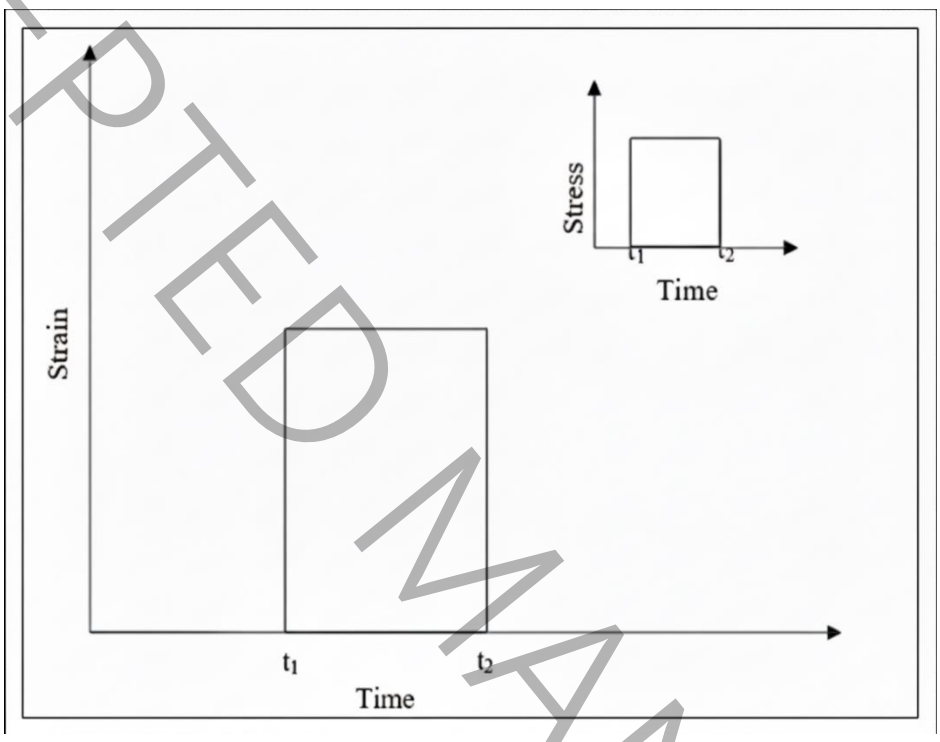

Figure 1: Schematic of step-strain and step-stress loading used in viscoelastic analysis (adapted from [12]).

For semi-crystalline and amorphous polymers such as PLA, strain-rate sensitivity arises from the interplay between viscoelastic and viscoplastic deformation mechanisms. At relatively low strain rates, molecular chains and entanglements have sufficient time to rearrange, so the material response is more compliant and ductile. As the strain rate increases, molecular relaxation is progressively suppressed, which leads to higher apparent stiffness and strength but also to reduced ductility and, in some cases, localized damage at interlayer interfaces in FDM-printed parts. At

even higher rates, limited heat dissipation can induce localized thermal softening while the bulk response still appears rate-strengthened. Recent experimental work on FDM-printed PLA confirms strong positive strain-rate sensitivity of tensile properties within the quasi-static regime investigated here. Asif et al reported significant dependence of silica reinforced 3D printed polymer on strain rates [13].

Although extensive research has been conducted on FDM-processed thermoplastics such as ABS, PC, ULTEM, and PPSF/PPSU, limited work specifically addresses the mechanical behavior of pure PLA fabricated using FDM. Prior studies have explored the influence of process parameters on the fatigue, tensile, flexural, and compressive properties of ABS components [14-18], as well as the dynamic mechanical characteristics of ABS-based prints [19, 20]. Similar investigations on PC, ULTEM, and PPSF/PPSU have examined their viscoelastic and mechanical performance under varying FDM settings [21-26].

In contrast, research on FDM-printed PLA is comparatively sparse. Most existing efforts focus on PLA composites [3, 4] or involve mechanical testing using modified printers like RepRap systems [27], rather than systematic evaluation of pure PLA under varying process conditions. Despite the growing adoption of PLA in additive manufacturing, a comprehensive understanding of its strain-rate-dependent properties and build orientation effects remains lacking.

Fused Deposition Modeling (FDM), a prominent rapid prototyping (RP) technique, builds 3D structures layer by layer directly from CAD input. While additive manufacturing initially gained traction with the introduction of stereolithography in 1986 [28], recent trends emphasize material characterization for FDM-printed thermoplastics [29-31]. However, PLA-specific data within this context is still limited.

A wide range of additive manufacturing (AM) processes—such as stereolithography (SLA), selective laser sintering (SLS), laminated object manufacturing (LOM), and three-dimensional printing (3DP)—are now available for producing polymeric and metallic components. Among these, fused deposition modeling (FDM) has become the most widely adopted method for polymer-based parts because of its low cost, modest equipment requirements, and ability to fabricate complex geometries directly from CAD models. In this work we focus specifically on FDM-printed PLA, as it combines the environmental benefits of a biobased polymer with the process-induced anisotropy and strain-rate sensitivity that are highly relevant for engineering and biomedical applications.

FDM-printed parts are inherently anisotropic, meaning their mechanical performance varies based on build orientation and raster angle. While materials like ABS and PC have been extensively characterized for such dependencies, the mechanical behavior of PLA under different strain rates and build parameters is still not comprehensively understood [31, 32]. In contrast, SLA uses a laser to cure liquid photopolymers [28, 32] and SLS fuses powdered materials without the need for support structures [33-35], offering high resolution but at higher cost and complexity. LOM, on the other hand, relies on laminated sheets bonded via thermal adhesive and are used primarily for visual models or tooling [36, 37].

PLA is widely adopted in FDM because of its ease of printing, dimensional stability, and relatively low material cost. Unlike ABS—which generally provides higher impact resistance and better thermal stability—PLA offers higher stiffness but lower ductility and a lower heat deflection temperature. As a result, neat PLA is commonly used for consumer products, packaging, prototyping, and low-to-moderate mechanical load applications, while PLA composites or

engineering polymers are preferred for more demanding environments. The mechanical and thermal characteristics relevant to this study are summarized in Table 1.

Table 1 Key mechanical and thermal properties of polylactic acid (PLA).

Property	Typical Value	Reference
Tensile strength	50–70 MPa	Ajioka et al. (1995)
Young's modulus	2.7–3.5 GPa	Ajioka et al. (1995)
Elongation at break	3–6%	Lunt (1998)
Glass transition temperature (Tg)	55–65 °C	Lunt (1998)
Melting temperature (Tm)	130–180 °C	Lunt (1998)

Thermoplastics have gained popularity due to their lightweight nature, cost-effectiveness, and ability to form complex geometries. Over the past four decades, their use in structural applications has grown, despite earlier perceptions of their mechanical inferiority to metals. Since the 1980s, low-cost polymers have been increasingly adopted in consumer and automotive sectors. While thermoplastics are commonly used in engineering for load-bearing elements in industry [38] and now their applications extend to biomedical and tissue engineering with innovations like scaffold designs [39] and knotless suture anchors [40]. Recent research also focuses on enhancing FDM thermoplastics for advanced uses such as electromagnetic and X-ray shielding [41].

This study aims to investigate the mechanical behavior of polylactic acid (PLA) components fabricated using fused deposition modeling (FDM) under varying process conditions. Specifically, it examines the influence of build orientation, raster angle, infill pattern, and strain rate on tensile strength, strain response, and failure behavior. The objective is to identify optimal FDM parameters that enhance the mechanical performance of PLA parts. Additionally, the study

integrates experimental testing with finite element simulations using Ansys and Abaqus to validate and interpret stress–strain responses under different conditions.

2. Methodology

This section outlines the sample preparation and testing procedures used in the investigation. Test specimens were fabricated using Ender 3 Pro and Xplorer 3D FDM printers with PLA reels, employing three different build orientations. In the FDM process, semi-molten PLA was extruded through a nozzle and deposited layer by layer to form the samples. The three construction orientations were chosen to study their influence on the mechanical behavior of the printed PLA parts.

2.1 Materials

In this study, commercial 1.75 mm-diameter PLA filament (red, nominal diameter tolerance ±0.05 mm) was used to fabricate all specimens by FDM. According to the supplier and the engineering data library used in ANSYS, PLA has a density of approximately 1250 $kg \cdot m^{-3}$ and a Young's modulus of about 3.4 GPa, with Poisson's ratio ≈0.39 (see Table 4). These values are consistent with those reported for neat PLA in the literature and were used as input for the numerical simulations. No additional fillers or modifiers were added to the filament.

2.2 Xplorer 3D and Ender 3 pro FDM Machines

Both printers used in this study employed the fused deposition modeling (FDM) technique. The Ender 3 Pro (Creality, China) has a build volume of 220 × 220 × 250 mm and a single 0.4 mm nozzle, while the Xplorer 3D printer (Pakistan) provides a build volume of 200 × 200 × 180 mm with the same nozzle diameter. In all experiments the extruder temperature was set to 220 °C and the bed temperature to 45 °C, which are within the recommended processing window for PLA and

ensure stable filament extrusion. Other machine features (user interface, electronics, etc.) are standard for desktop FDM systems and are not expected to influence the mechanical behavior of the printed specimens.

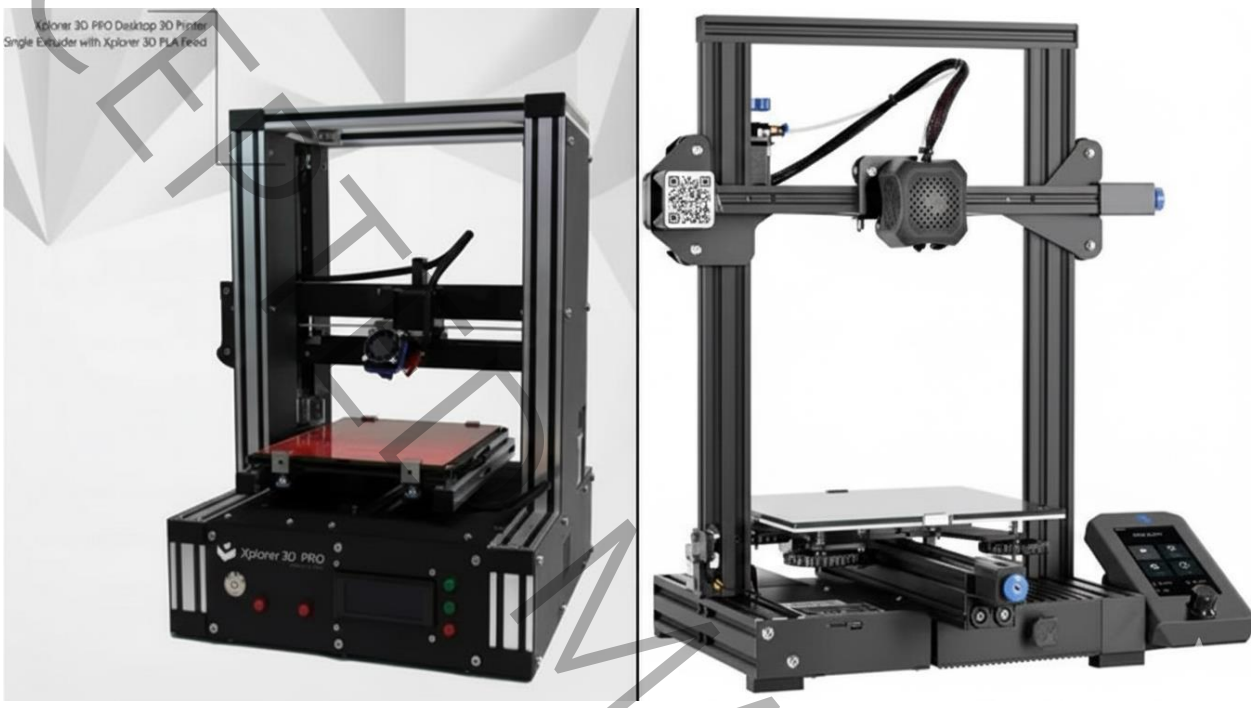

Figure 2: Xplorer 3D and Ender 3 Pro FDM machines used in this study. The Ender 3 Pro has a build volume of 220 × 220 × 250 mm, and the Xplorer 3D machine has a build volume of 200 × 200 × 180 mm, which provides dimensional scale for the figure.

Fused Deposition Modeling (FDM), a material extrusion additive manufacturing technique, uses polymer filament that is heated to a molten state and extruded through a 3D printer nozzle. The nozzle moves in three degrees of freedom (DoF) to deposit material on the build plate according to G-code instructions. Continuous filament feeding is achieved using two counter-rotating rollers that push the material through the extruder. The object is formed layer by layer until the final shape and size are completed [42].

2.3 Part fabrication

FDM printers were used to fabricate "dog-bone" shaped specimens for tensile testing based on ASTM D638 Type V standards, commonly used for evaluating plastic material properties (see Figure 3). The geometry of each specimen was measured as per the standard to investigate its tensile behavior. All specimens were printed with a 0.4 mm nozzle, 0.10 mm layer height, 100 % infill density, 0.5 mm nominal shell thickness, a nozzle temperature of 220 °C, and a bed temperature of 45 °C, as summarized in Table 2. These standardized samples are widely accepted in research for consistent mechanical testing. Each specimen weighed approximately 2 grams and required 16 minutes to print using the specified parameters. Table 2 lists the full set of slicing and printing parameters used for all specimens, including nozzle diameter, layer height, shell thickness, infill density, printing speed, and nozzle/bed temperatures.

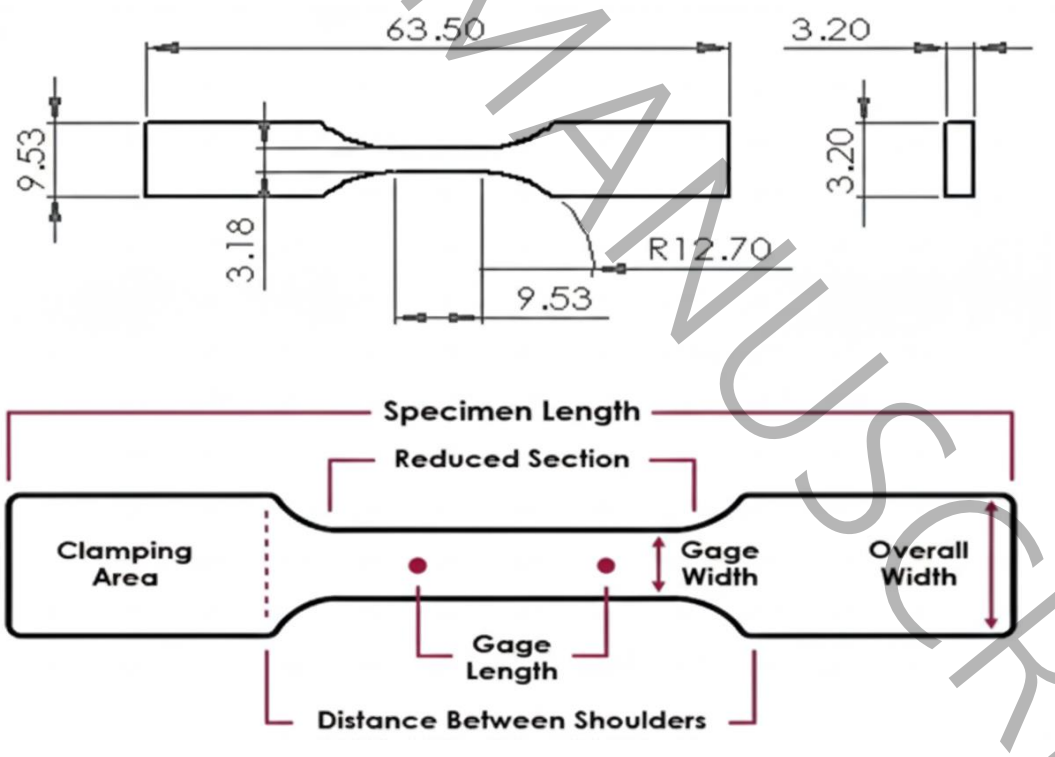

Figure 3: ASTM D638 Type-V & Dog-Bone specimen geometry.

Table 1: Printing parameters.

Machine	
Nozzle size (mm)	0.4
Retraction	
Speed (mm/s)	40.0
Distance (mm)	4.5
Quality	
Initial layer thickness (mm)	0.3
Initial layer line width (%)	100
Cut off object bottom (mm)	0.0
Dual extrusion overlap (mm)	0.15
Speed	
Travel speed (mm/s)	150.0
Bottom layer speed (mm/s)	20
Infill speed (mm/s)	0.0
Outer shell speed (mm/s)	0.0
Inner shell speed (mm/s)	0.0
Cool	
Minimal layer time (s)	5
Enable cooling fan	Yes
Quality	
Layer height (mm)	0.1
Shell Thickness (mm)	0.5
Enable retraction	Yes
Fill	

Bottom/Top thickness (mm)	0.4
Fill Density (%)	100
Speed and Temperature	
Print speed (mm/s)	50
Printing temperature (C)	220
Bed temperature(C)	45
Support	
Support type	None
Platform Adhesion type	None
Filament	
Diameter (mm)	1.75
Flow (%)	100.0

2.4 Experimentation

The experimental program comprised two main studies:

1. Study the effect under different strain rates
2. Study the effect under different orientation, and raster angles

In the first phase of our study, we selected three crosshead speeds—2 mm/s, 5 mm/s, and 10 mm/s—which correspond to quasi-static engineering strain rates in the range typically used for polymer tensile tests and for recent investigations of strain-rate sensitivity in FDM-printed PLA. For each strain rate, three independent tensile tests were conducted (n = 3), and the average of the three measurements was taken to minimize the influence of random human and machine error. **Table 3** outlines the testing methodology. A Universal Testing Machine (UTM) was used, which involves pulling a prepared specimen until fracture to evaluate its load response. The process included specimen mounting, zeroing, calibration, and setting parameters like crosshead speed and

gauge length. During testing, the UTM recorded load, displacement, and time, and the resulting stress-strain data was analyzed to determine key mechanical properties relevant to the study. See **Figure 11** for experimental samples. After printing, all specimens were stored under ambient laboratory conditions (approximately 25 ± 2 °C) for at least 24 hours prior to mechanical testing. No additional drying, annealing, or humidity conditioning was applied, and specimens were tested in the as-printed state.

Table 2: Experimental parameters used for present study.

Strain Rate (mm/s)	Build Orientation	Raster Angle (°)	Infill Pattern	No. of Samples
1	0°	0	Concentric	3
1	90°	15	Hexagonal	3
1	On Edge	45	Concentric	3
5	0°	0	Hexagonal	3
5	90°	15	Concentric	3
5	On Edge	45	Hexagonal	3
10	0°	0	Concentric	3
10	90°	15	Hexagonal	3
10	On Edge	45	Concentric	3

For all strain-rate experiments, specimens were printed with 0° raster angle, flat (0°) orientation, and concentric infill. These settings were intentionally held constant to isolate the effect of strain rate without introducing variability from geometry-dependent parameters. For the orientation, raster angle, and infill pattern studies, the strain rate was fixed at 5 mm/s to ensure comparability across configurations. All samples were printed using identical layer height (0.1 mm), nozzle temperature (220°C), bed temperature (45°C), and infill density (100%). Only one

parameter was varied at a time while others were kept constant. The second phase of our study focuses on evaluating the tensile properties of specimens by varying the build orientation, raster angle, and infill pattern. Like the first phase, each combination of build orientation, raster angle, and infill pattern was tested using three replicate specimens (n = 3), and the average values are reported. Because only averaged values were retained in the research study records, retrospective calculation of standard deviation or ANOVA was not possible. The averaged results nevertheless allow clear comparison of trends among the tested printing parameters. The experimental setup and corresponding parameters are detailed in the tables provided below, See **Figure 4**.

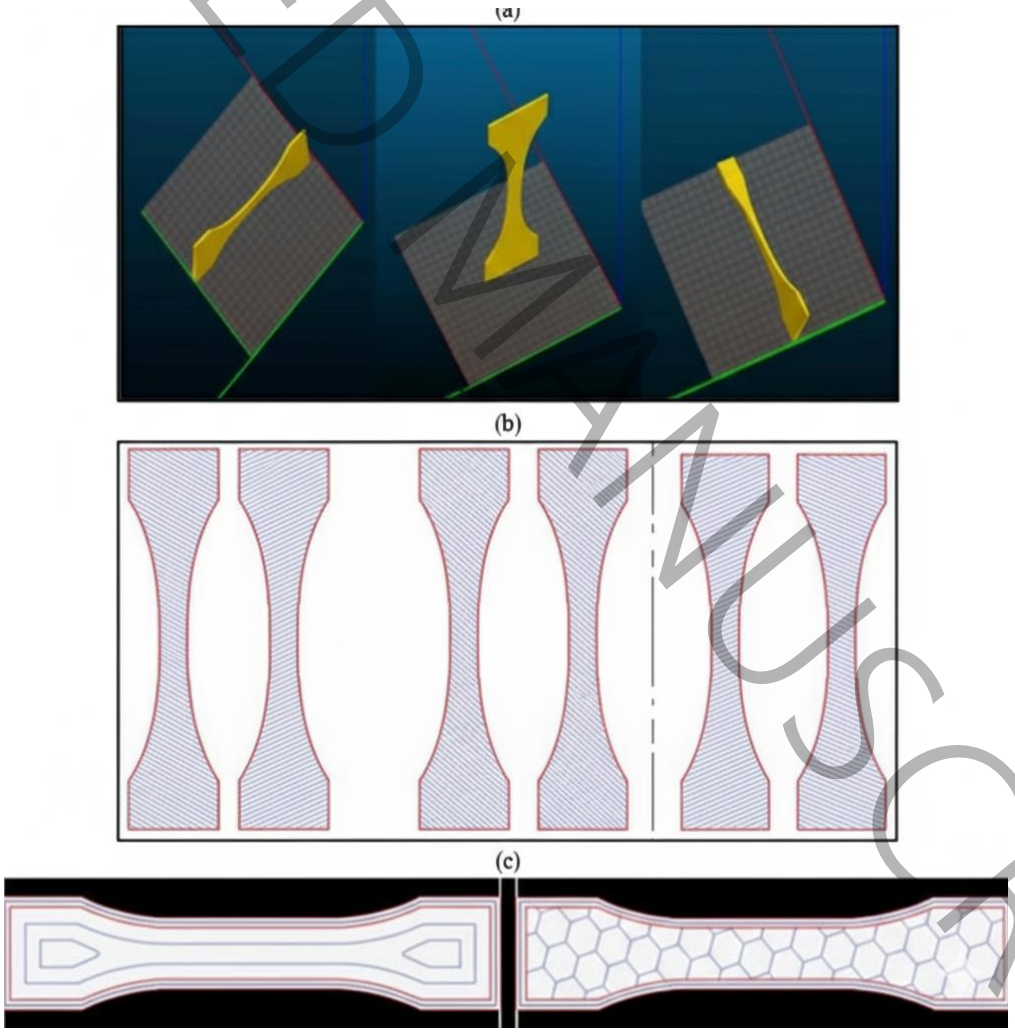

Figure 4: Printing parameters - (a) Orientations, (b) Raster angles, and (c) Infill patterns.

2.5 Numerical Analysis

In the numerical analysis phase, we employed ANSYS 23 (R2) Explicit Dynamics to simulate the tensile tests with prescribed end velocities and Abaqus 23 for complementary parametric studies, as both software packages are widely used to model the mechanical response of FDM-printed polymers under rate-dependent loading. A CAD model of the dog-bone specimen, based on ASTM D638 standards, will be created in the design modeler. The resulting stress-strain curves from the simulations will be validated against the experimental data to ensure accuracy. The specimen was meshed with 0.5 mm linear brick elements, which offered a practical balance between accuracy and computational cost; a more detailed mesh-convergence study is acknowledged as an important topic for future work. See Figure 5.

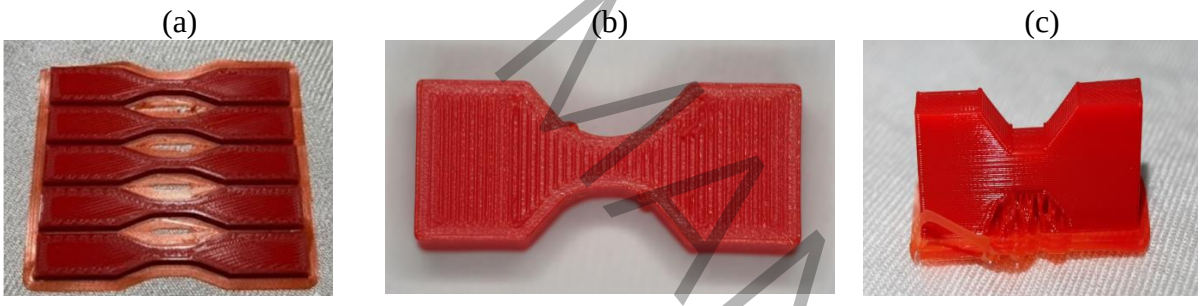

Figure 5: Live printed ASTM D638 Type-V tensile specimens: (a) 15° raster angle, (b) X-orientation, and (c) on-edge configuration with support structure. Each specimen follows the ASTM D638 Type-V geometry with an overall length of 63.5 mm, gauge length of 7.62 mm, and narrows-section width of 3.18 mm, which provides dimensional scale for the images.

3. Results and Discussions

3.1 Strain Rate Dependent Study

In this study we aimed to numerically and experimentally validate our findings. For experimental work we used Tinius Olsen UTM with a load cell of 50 KN, clamped our specimen

from both sides and applied deformation rates (2mm/s, 5mm/s, 10mm/s), and by the aid of Olsen navigator software we were able to get the load-deformation readings which were later converted to stress and strain values. These crosshead speeds fall within the quasi-static strain-rate range recommended for polymer tensile testing and are consistent with recent experimental studies on the rate-dependent tensile and thermomechanical behavior of FDM-printed PLA, making them relevant to typical service conditions for structural and biomedical components rather than extreme impact loading.

As for the numerical validation, we used Ansys software (v 19 R3). In this we sketched our specimen in its design modeler, later applied boundary conditions (fixed support on one end, deformation velocity at the other). Deformation velocity here refers to the speed at which the jaws of the UTM were being operated. Subsequently ran the simulation on the above-mentioned velocities. Each simulation required approximately 10 to 15 hours to complete. See **Figure 9**.

3.2 Numerical Modeling

Figure 6 illustrated the experimental setup used for mechanical testing of the PLA specimens. Subfigure (a) shows the Universal Testing Machine (UTM) by Tinius Olsen, which applies controlled tensile force to the specimen. Subfigure (b) provides a close-up view of the dog-bone-shaped PLA specimen securely clamped within the machine's jaws. This setup is critical for evaluating stress-strain behavior under different printing and loading conditions. See Table 4 for PLA material properties.

Figure 7 displayed the geometry of the dog-bone tensile specimen created using the Design Modeler module in ANSYS. The model precisely replicates the physical dimensions used in the experimental setup for accurate simulation results.

Figure 8 showed the boundary conditions applied in ANSYS Mechanical during the explicit

dynamic simulation. One end of the specimen is fixed to mimic clamping, while the other end is subjected to a predefined velocity load to simulate tensile stress. This setup enables the analysis of mechanical behavior under realistic strain conditions.

Figure 9 illustrated the simulation results for the tensile specimen subjected to a strain rate of 10 mm/s using ANSYS Explicit Dynamics. The top image shows the equivalent (von Mises) stress distribution, with maximum stress concentrated in the necked region (red zone), indicating the most likely fracture point. The bottom image displays the corresponding equivalent strain distribution, showing uniform deformation across the reduced section with peak strain occurring centrally. These results validate the mechanical response of PLA under high strain rate loading and help correlate with experimental findings.

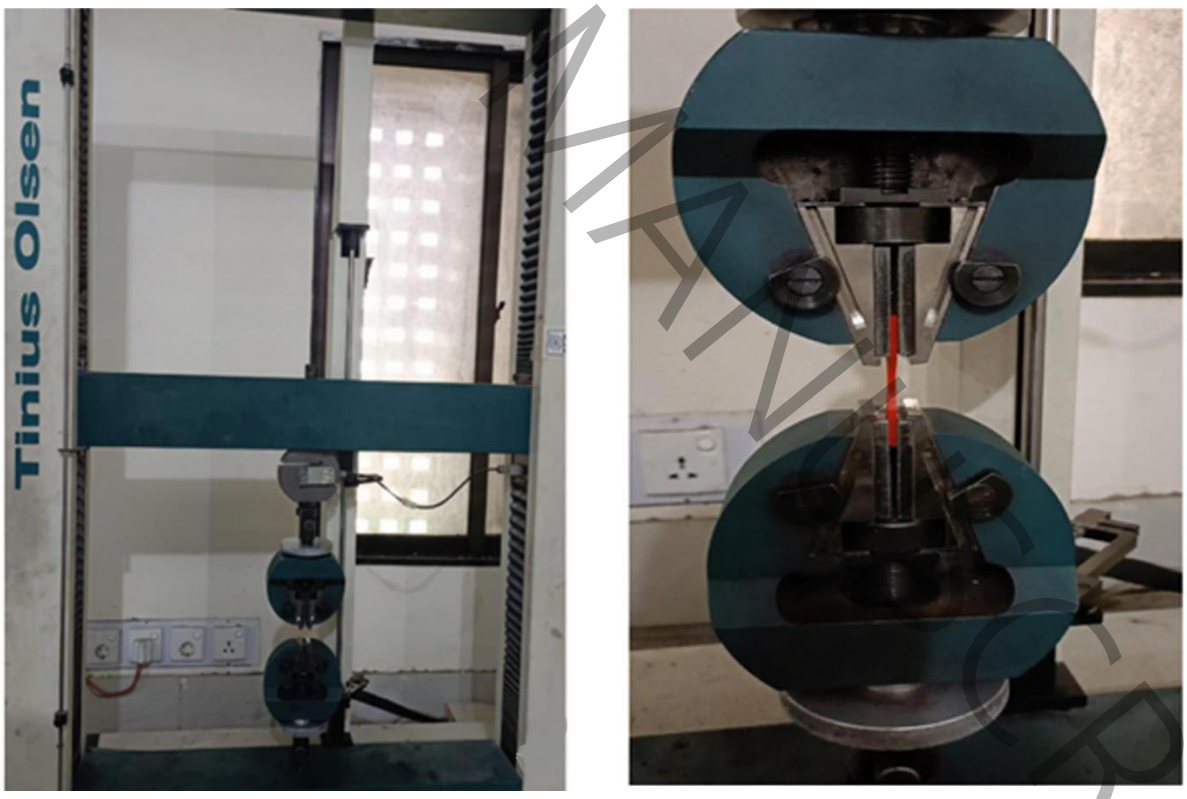

(a) (b)

Figure 6: (a) UTM, (b) Specimen clamped in jaws

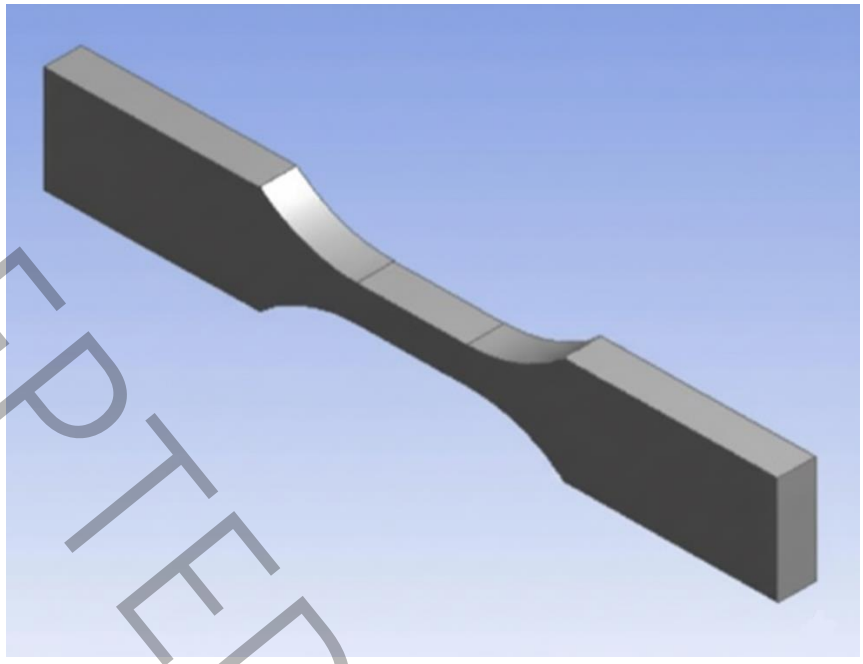

Figure 7: Design modeler

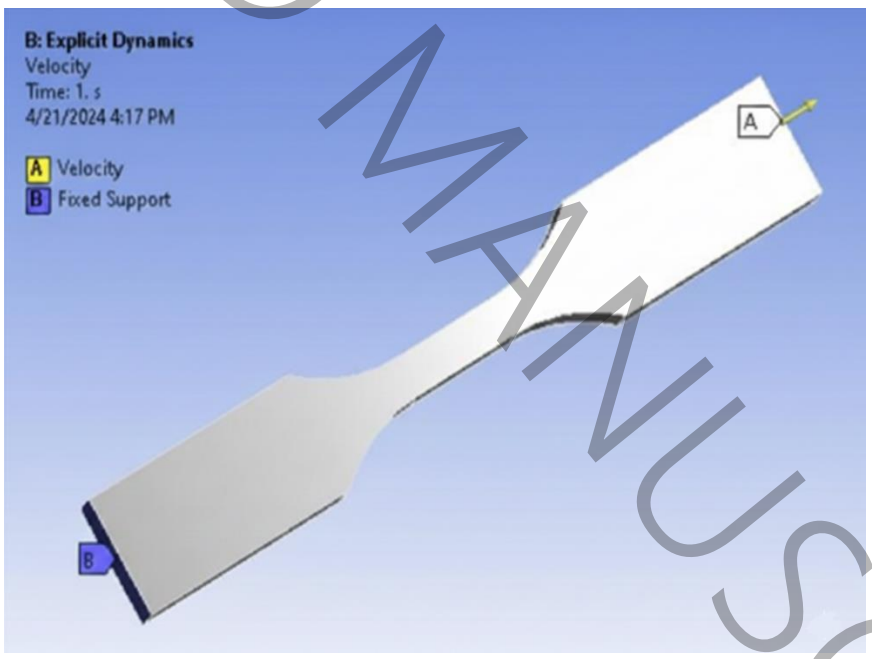

Figure 8: ANSYS mechanical

Table 3: Material properties of polylactic acid (PLA)

Property	Value	Unit
Density	1250	$kg \cdot m^{-3}$
Coefficient of Thermal Expansion	0.000135	$°C^{-1}$
Isotropic Elasticity		

– Young's Modulus	3.45×10^9	Pa
– Poisson's Ratio	0.39	–
– Bulk Modulus	5.2273×10^9	Pa
– Shear Modulus	1.241×10^9	Pa
Tensile Yield Strength	5.41×10^7	Pa
Tensile Ultimate Strength	5.92×10^7	Pa
Specific Heat Capacity, C_p	1190	$J \cdot kg^{-1} \cdot °C^{-1}$

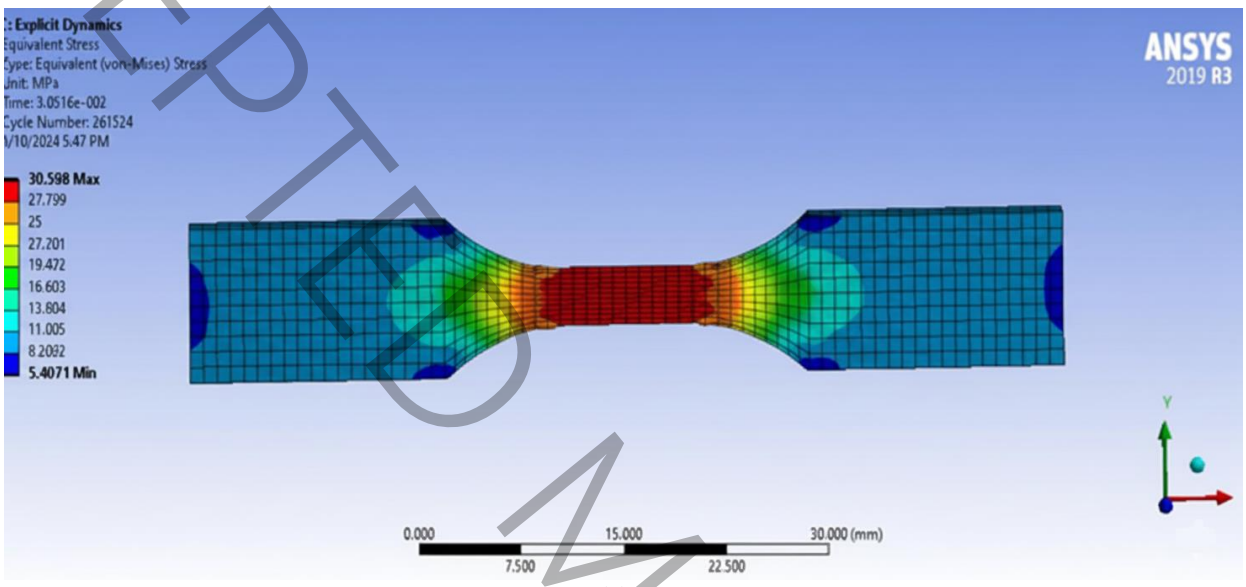

(a)

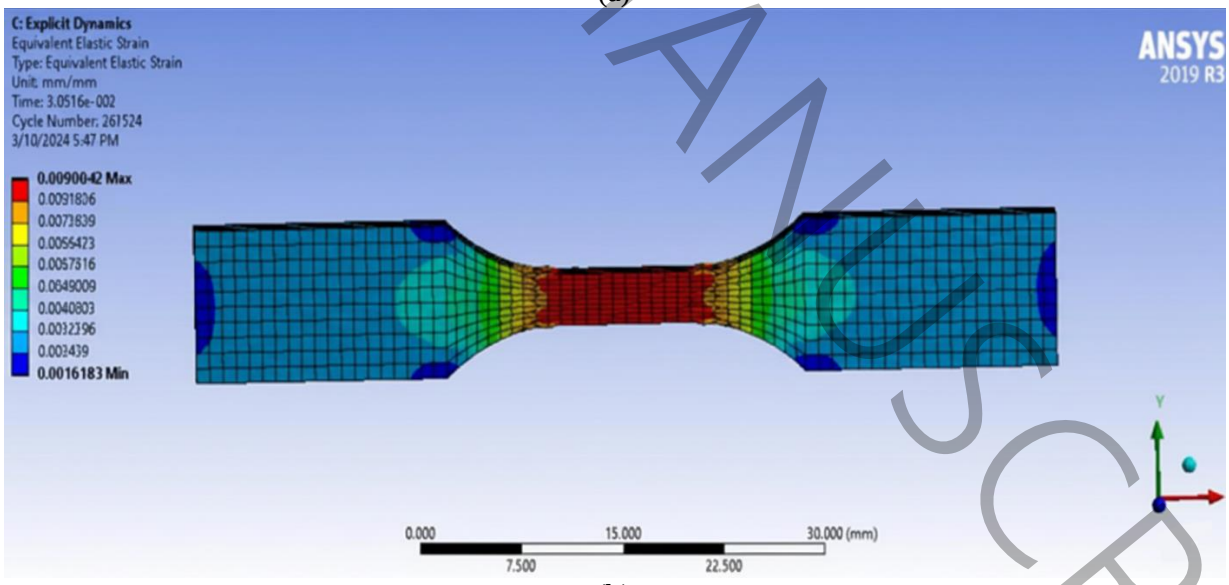

(b)

Figure 9: Simulation output - Equivalent stress and strain at 10 mm/s.

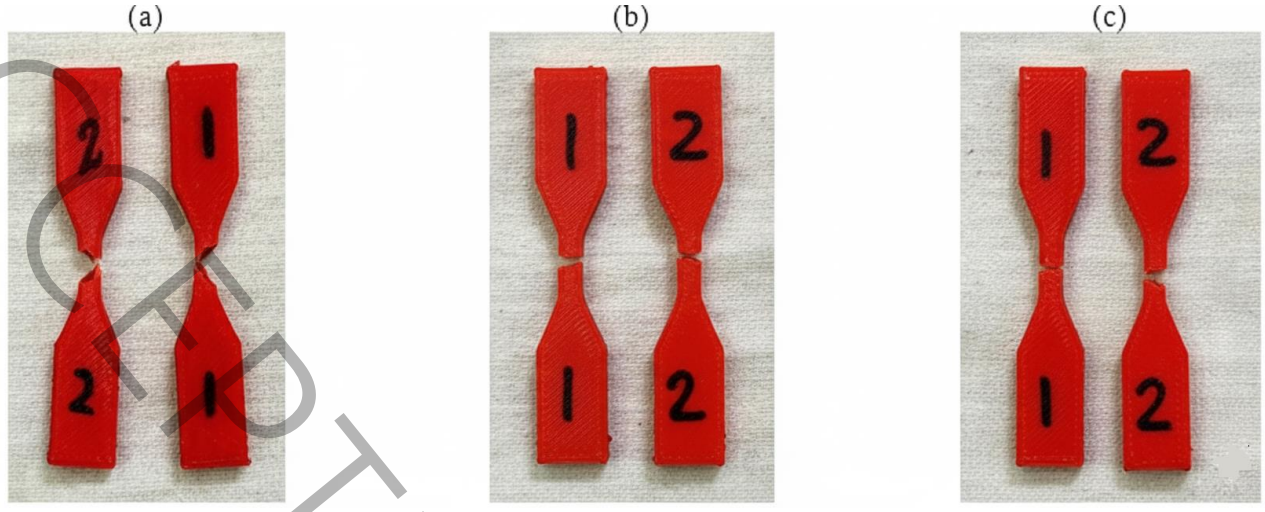

Figure 10: Experimental samples at (a) 2mm/s, (b) 5mm/s, and (c) 10mm/s, respectively.

To quantify the level of agreement between the simulations and the experiments, the maximum stresses and corresponding strains extracted from the ANSYS results were next compared with the experimental tensile data in the form of stress–strain curves, as presented in Figures 11–13.

Figure 11: Graphical comparison for 2mm/s.

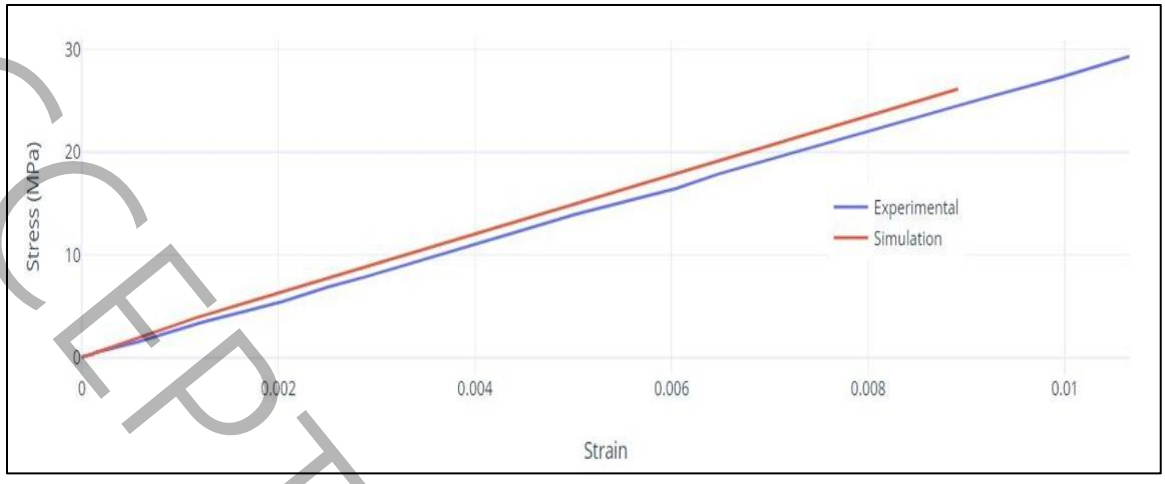

Figure12: Graphical comparison for 5mm/s.

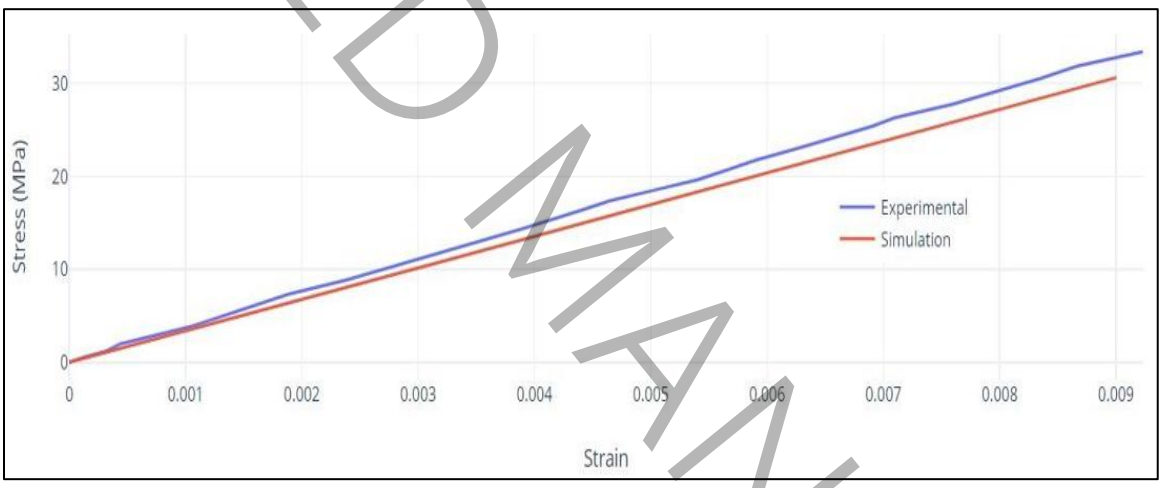

Figure 13: Graphical comparison for 10mm/s.

Figures 11–13 demonstrate that both the experimental and numerical stress–strain curves are approximately linear over the investigated strain range. The maximum values for stress and strain are mentioned in **Table 5**. At the lowest strain rate of 2 mm/s, both the peak stress and failure strain were lower because PLA exhibits characteristic viscoelastic behavior. At slow loading rates, polymer chains have more time to relax and reorient, which reduces the effective stiffness and delays load transfer within the material. As a result, the material responds more compliantly,

producing lower stress values and higher deformation before significant strain hardening occurs. This trend is widely reported for PLA and other thermoplastic polymers under quasi-static loading, where increased molecular mobility at low strain rates leads to reduced tensile strength.

Table 4: Maximum stress and strain values.

Velocity (mm/s)	Analysis	Stress (MPa)	Strain
2	Experimental	15.483	0.004064
	Simulation	13.098	0.003823
5	Experimental	29.318	0.010659
	Simulation	26.13	0.008915
10	Experimental	33.386	0.009232
	Simulation	30.598	0.009004

For the 10 mm/s case (Figure 13), the experimental stress exceeded simulation predictions. This difference arises from small dimensional deviations in FDM-printed samples, particularly neck-width variations identified during measurement (±0.12 mm). Such deviations increase the effective load-bearing cross-section, leading to higher measured stresses compared to the idealized CAD geometry used in simulation.

When utilizing PLA as our FDM printed material for evaluating strain rate-dependent mechanical behavior, you may better understand why our simulation and experimental findings showed a linear trend by considering these components and their corresponding numerical ranges. As shown in Table 5, there is a systematic deviation between the experimental and numerical stress values, with experiments yielding slightly higher peak stresses for all three deformation rates. This discrepancy likely arises from a combination of factors. First, the printed specimens inevitably exhibit small deviations from the ideal ASTM D638 Type-V geometry, whereas the finite element

model strictly follows the nominal dimensions. Second, the numerical model employs a simplified, homogeneous material description and does not explicitly represent interlayer voids or imperfect bonding, which can alter the effective stiffness of FDM-printed PLA. Finally, frictional effects at the grips and any minor misalignments are present in the physical tests but not in the simulations. Because a full quantitative dimensional survey of all specimens relative to ASTM tolerances was not carried out, we have refrained from attributing the discrepancy solely to dimensional inaccuracy and instead acknowledge it as an interplay of geometric and modeling simplifications.

3.3 Raster angle builds orientation and infill pattern

3.3.1 Raster angle

For every filament, 0° raster orientation showed the maximum UTS, which steadily dropped as the angle increased. The rationale is because the filament bears the tensile stress at 0°, but when the raster orientation shifts to 45°, the bond strength—which is weaker— becomes more significant in determining the total strength. This work is similar with that of [43], who likewise noted a steady decline in UTS values for PLA filament intermediate raster angle values. It matters which way the layers are oriented in relation to the force exerted. The layers can bear the force more efficiently when it is applied along the X-axis, which is parallel to the infill lines at a 0-degree angle. This is because the layers are piled vertically. Conversely, when the tensile force is applied along the Y-axis, which is 45 degrees parallel to the infill lines, the layers are stacked horizontally, which might facilitate the separation of layers under stress. Pattern and Density of Infill: Generally speaking, a 0-degree raster angle is equivalent to a higher infill density (like 100%) than a 45-degree angle. Because there is more material to distribute load and resist deformation, printers with a higher infill density often have stronger constructions [44]. See **Figure 14** and **Table 6** for raster angle details.

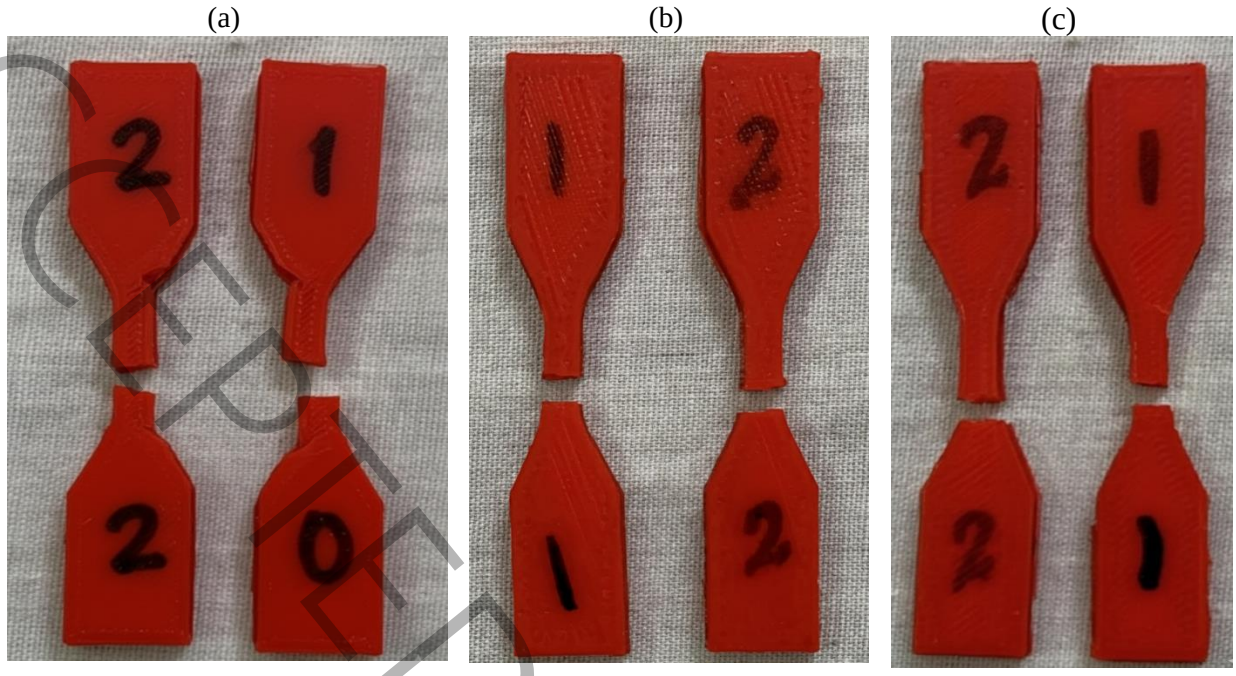

Figure 14: Raster angles.

Table 5: Raster angle details.

Raster Angle	Stress (MPa)
0°	36.25
15°	34.6
45°	31.2

The tensile stress results demonstrated a clear decline as the raster angle increased from 0° to 45°. At 0°, the stress reached 36.25 MPa, dropping to 34.6 MPa at 15°, and further to 31.2 MPa at 45°. This trend aligns with observations by Lanzotti et al [43], who showed that a 0° raster angle—where filament orientation matches the tensile loading direction—enhances load transfer and stress-bearing capacity due to improved filament continuity. Cakan [44] also reported that higher raster angles introduce more cross-sectional discontinuities, weakening the internal bond structure and leading to earlier failure. Our data validates these prior findings, indicating that aligning raster paths with the loading axis significantly improves mechanical strength in FDM-printed PLA

specimens. From a microstructural perspective, roads printed at 0° act as nearly continuous fibers along the loading axis, so the applied tensile stress is carried primarily by the bulk PLA within each filament. At higher raster angles, the load must be transferred across a larger number of interroad interfaces and small voids, which behave as stress concentrators and preferred crack-initiation sites. Finite element microstructural models and fractographic observations reported in the literature support this mechanism, showing that failure at high raster angles is dominated by debonding and coalescence of these interfacial defects rather than by yielding of the filament cores.

3.3.2 Printing orientation

Compared to specimens printed in 90-degree orientations, those printed in 0° orientation had the maximum tensile strength for PLA. This outcome can be ascribed to the 0° orientation used in the layer-by-layer construction, which most likely improved interlayer adhesion and decreased the number of weak spots along the print lines [45]. See **Figure 15** and **Table 7** for printing orientations.

The tensile stress results reveal a significant dependency on build orientation. The sample printed on edge exhibited the highest tensile stress of 32.3 MPa, followed closely by the 0° orientation at 31.2 MPa, while the 90° orientation demonstrated the lowest value of 22.5 MPa. This noticeable reduction in stress for vertically printed (90°) samples corresponds with findings by [14], [45], who highlighted that layer interfaces perpendicular to the loading direction act as stress concentrators, leading to poor interlayer adhesion and early failure. In contrast, horizontal and edge builds exhibit stronger layer cohesion along the tensile axis, enabling better load transfer and structural integrity. These results confirm the importance of optimizing build orientation to achieve maximum mechanical strength in FDM-printed PLA components.

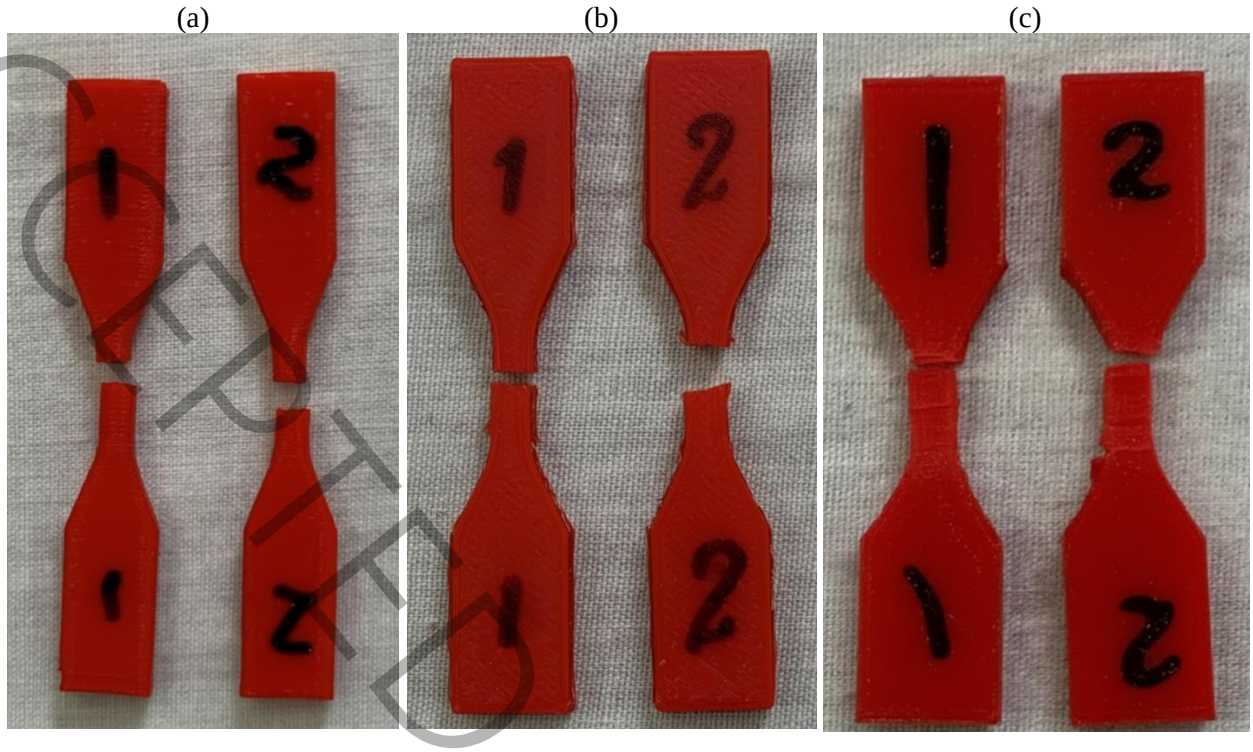

Figure 15: Printing orientation.

Table 6: Printing orientation details.

Printing Orientation	Stress (MPa)
90°	22.5
0°	31.2
On Edge	32.3

3.3.3 Infill patterns

The results of the experiment showed that, in comparison to the grid and trihexagonal infill patterns, the concentric infill pattern had greater stress-strain values. With respect to printing orientation, the direction of the applied tensile force and the concentric infill pattern are aligned in the same way. It permits a greater force to be applied to the specimen before it fractures. With the applied load, however, the alignment of the trihexagonal and grid infill patterns differs. As a result,

the imposed load could not be evenly distributed throughout the entire body of the animal. The specimens become weaker than the concentric pattern as a result [46]. See **Figure 16** and **Table 8** for infill pattern detail.

(a) (b)

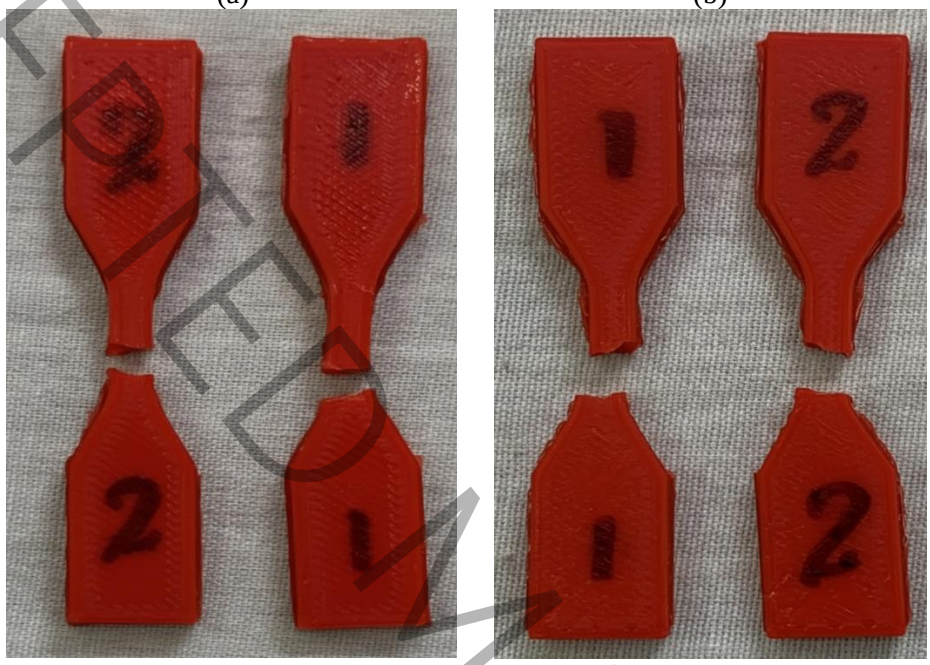

Figure16: Infill Pattern: (a) Concentric circle, (b) Hexagon

Table 7: Infill pattern detail

Infill Pattern	Stress (MPa)
Concentric Circle	26.4
Hexagon	20.2

Among the tested infill patterns, the concentric circle configuration exhibited a significantly higher tensile stress of 26.4 MPa compared to 20.2 MPa for the hexagonal pattern. This result supports findings by [47], who demonstrated that concentric infill improves mechanical performance by providing continuous load paths and reducing internal stress concentrations. In contrast, hexagonal patterns, though material-efficient, tend to introduce more internal voids and

stress risers, leading to earlier failure under tensile loading. It should be noted, however, that concentric infill generally requires slightly longer print times than simple line or hexagonal patterns at the same nominal infill density, because the toolpath includes multiple closed contours and frequent changes in direction. In addition, depending on slicer settings, concentric infill may result in similar or slightly higher material usage than hexagonal infill for the same nominal density. Designers must therefore weigh the observed mechanical benefits against potential penalties in build time and material consumption when selecting an infill strategy. These findings highlight that infill geometry has a measurable impact on structural performance, and concentric patterns are better suited when mechanical strength is a design priority in FDM-printed PLA components.

4. Conclusion

This study presented an experimental and numerical investigation of the strain-rate-dependent tensile behavior of FDM-printed PLA dog-bone specimens, with a particular focus on the influence of build orientation, raster angle, and infill pattern. Tensile tests conducted at crosshead speeds of 2, 5, and 10 mm/s showed a clear positive strain-rate sensitivity: the ultimate tensile stress increased by more than 100 % between the lowest and highest rates, whereas the failure strain decreased, indicating a transition toward more brittle behavior at higher loading rates.

The mechanical response was also strongly affected by printing orientation and raster angle. Specimens printed on edge and in the 0° raster condition exhibited the highest tensile strengths (up to 32.3 MPa), while vertically built (90°) and 45° raster specimens showed markedly lower strength due to weaker interlayer bonding and more unfavorable filament alignment. In

terms of infill pattern, concentric infill produced the highest tensile stress (26.4 MPa) compared with hexagonal infill (20.2 MPa), at the cost of somewhat longer print times.

Finite element simulations performed in ANSYS, using material properties consistent with the literature for neat PLA, reproduced the overall stress–strain trends and the relative influence of strain rate, although experimental peak stresses were slightly higher than the simulated values. This difference is attributed to a combination of geometric deviations from the ideal ASTM D638 profile and simplifications in the numerical material model. Overall, the level of agreement between experiments and simulations supports the use of relatively simple FE models as a first-order tool for predicting the tensile response of FDM-printed PLA parts.

From a design perspective, the results demonstrate that higher crosshead speeds, favorable build orientations (on edge or 0°), and concentric infill can substantially enhance the tensile performance of PLA components fabricated by FDM. These insights provide practical guidelines for selecting process parameters when PLA parts are intended for structural or biomedical applications operating under quasi-static tensile loading. Future work will extend the present study by incorporating more detailed constitutive models, mesh-convergence analyses, and temperature-dependent behavior to further improve the predictive capability for FDM-printed PLA. Typical application areas that can benefit from these findings include patient-specific orthoses and guides, small structural brackets, fixtures, and functional consumer products fabricated by FDM-printed PLA.

Conflicts of Interest: The authors declare no conflicts of interest.

5. References

[1] S. Freinkel, A brief history of plastic's conquest of the world, Sci Am, (2011).
[2] M. Jamshidian, E.A. Tehrany, M. Imran, M. Jacquot, S. Desobry, Poly-lactic acid: production, applications, nanocomposites, and release studies, Comprehensive reviews in food science and food safety, 9(5) (2010) 552-571.

[3] Y. Dong, A. Ghataura, H. Takagi, H.J. Haroosh, A.N. Nakagaito, K.-T. Lau, Polylactic acid (PLA) biocomposites reinforced with coir fibres: Evaluation of mechanical performance and multifunctional properties, Composites Part A: Applied Science and Manufacturing, 63 (2014) 76-84.
[4] T. Kasuga, Y. Ota, M. Nogami, Y. Abe, Preparation and mechanical properties of polylactic acid composites containing hydroxyapatite fibers, Biomaterials, 22(1) (2000) 19-23.
[5] J.Y. Lim, S.H. Kim, S. Lim, Y.H. Kim, Improvement of Flexural Strengths of Poly (L-lactic acid) by Solid-State Extrusion, 2. Extrusion through Rectangular Die, Macromolecular Materials and Engineering, 288(1) (2003) 50-57.
[6] T. Furukawa, H. Sato, R. Murakami, J. Zhang, Y.-X. Duan, I. Noda, S. Ochiai, Y. Ozaki, Structure, dispersibility, and crystallinity of poly (hydroxybutyrate)/poly (L-lactic acid) blends studied by FT-IR microspectroscopy and differential scanning calorimetry, Macromolecules, 38(15) (2005) 6445-6454.
[7] C.A. Mills, M. Navarro, E. Engel, E. Martinez, M.P. Ginebra, J. Planell, A. Errachid, J. Samitier, Transparent micro-and nanopatterned poly (lactic acid) for biomedical applications, Journal of Biomedical Materials Research Part A: An Official Journal of The Society for Biomaterials, The Japanese Society for Biomaterials, and The Australian Society for Biomaterials and the Korean Society for Biomaterials, 76(4) (2006) 781-787.
[8] L.-T. Lim, R. Auras, M. Rubino, Processing technologies for poly (lactic acid), Progress in polymer science, 33(8) (2008) 820-852.
[9] G. Graefe, Holten, CH: Lactic Acid, Properties and Chemistry of Lactic Acid and Derivatives (Milchsäure, Eigenschaften und Chemie der Milchsäure und ihrer Derivate). With Contributions by A. Müller (Analytical Chemistry), D. Rehbinder (Biochemistry). Edited by Stichting ILRA–International Research Association, Kopenhagen. Verlag Chemie GmbH, Weinheim 1971. 566 Seiten mit 98 Abb. und 181 Tab., Englisch, Leinen DM 135,—, in, Wiley Online Library, 1973.
[10] J. Lunt, Large-scale production, properties and commercial applications of polylactic acid polymers, Polymer degradation and stability, 59(1-3) (1998) 145-152.
[11] D.E. Henton, P. Gruber, J. Lunt, J. Randall, Polylactic acid technology, in: Natural fibers, biopolymers, and biocomposites, CRC Press, 2005, pp. 559-607.
[12] W. Finley, J. Lai, K. Onaran, Creep and Relaxation of Nonlinear Viscoelastic Material, in, Netherland, North Holland Publishing Company, 1976.
[13] M. Asif, M. Ramezani, K.A. Khan, M.A. Khan, K.C. Aw, Investigation of the strain-rate-dependent mechanical behavior of a photopolymer matrix composite with fumed nano-silica filler, Polymer Engineering & Science, 59(8) (2019) 1695-1700.
[14] S.H. Ahn, M. Montero, D. Odell, S. Roundy, P.K. Wright, Anisotropic material properties of fused deposition modeling ABS, Rapid prototyping journal, 8(4) (2002) 248-257.
[15] A. Bellini, S. Güçeri, Mechanical characterization of parts fabricated using fused deposition modeling, Rapid Prototyping Journal, 9(4) (2003) 252-264.
[16] B.H. Lee, J. Abdullah, Z.A. Khan, Optimization of rapid prototyping parameters for production of flexible ABS object, Journal of materials processing technology, 169(1) (2005) 54-61.
[17] J. Lee, A. Huang, Fatigue analysis of FDM materials, Rapid prototyping journal, 19(4) (2013) 291-299.
[18] S.B. Mishra, S.S. Mahapatra, Improvement in tensile strength of FDM built parts by parametric control, Applied Mechanics and Materials, 592 (2014) 1075-1079.
[19] A. Arivazhagan, S. Masood, Dynamic mechanical properties of ABS material processed by fused deposition modelling, Int. J. Eng. Res. Appl, 2(3) (2012) 2009-2014.
[20] Z. Weng, J. Wang, T. Senthil, L. Wu, Mechanical and thermal properties of ABS/montmorillonite nanocomposites for fused deposition modeling 3D printing, Materials & Design, 102 (2016) 276-283.

[21] A. Arivazhagan, S. Masood, I. Sbarski, Dynamic mechanical analysis of fused deposition modelling processed polycarbonate, in: Annual Technical Conference-ANTEC, Conference Proceedings, 2011, pp. 950-955.
[22] A. Arivazhagan, A. Saleem, S. Masood, M. Nikzad, K. Jagadeesh, Study of dynamic mechanical properties of fused deposition modelling processed ULTEM material, American Journal of Engineering and Applied Sciences, 7(3) (2014) 307.
[23] V. Schöppner, K.P. KTP, Mechanical properties of fused deposition modeling parts manufactured with Ultem* 9085, in: Proceedings of the 69th Annual Technical Conference of the Society of Plastics Engineers (ANTEC'11), Boston, MA, USA, 2011, pp. 1-5.
[24] M. Domingo-Espin, S. Borros, N. Agullo, A.-A. Garcia-Granada, G. Reyes, Influence of building parameters on the dynamic mechanical properties of polycarbonate fused deposition modeling parts, 3D Printing and Additive Manufacturing, 1(2) (2014) 70-77.
[25] B. Huang, S. Masood, M. Nikzad, P.R. Venugopal, A. Arivazhagan, Dynamic mechanical properties of fused deposition modelling processed polyphenylsulfone material, (2015).
[26] S.H. Masood, K. Mau, W. Song, Tensile properties of processed FDM polycarbonate material, in: Materials science forum, Trans Tech Publ, 2010, pp. 2556-2559.
[27] B. Tymrak, M. Kreiger, J.M. Pearce, Mechanical properties of components fabricated with open-source 3-D printers under realistic environmental conditions, Materials & Design, 58 (2014) 242-246.
[28] R. Ramli, C. Lee, M. Kassim, Extraction and characterization of starch from microalgae and comparison with commercial corn starch, in: IOP conference series: Materials science and engineering, IOP Publishing, 2020, pp. 012012.
[29] S.A. Yavari, R. Wauthlé, J. van der Stok, A. Riemslag, M. Janssen, M. Mulier, J.-P. Kruth, J. Schrooten, H. Weinans, A.A. Zadpoor, Fatigue behavior of porous biomaterials manufactured using selective laser melting, Materials Science and Engineering: C, 33(8) (2013) 4849-4858.
[30] E. Brandl, U. Heckenberger, V. Holzinger, D. Buchbinder, Additive manufactured AlSi10Mg samples using Selective Laser Melting (SLM): Microstructure, high cycle fatigue, and fracture behavior, Materials & Design, 34 (2012) 159-169.
[31] N. Shamsaei, J. Simsiriwong, Fatigue behaviour of additively-manufactured metallic parts, Procedia Structural Integrity, 7 (2017) 3-10.
[32] K.G. Swift, J.D. Booker, Manufacturing process selection handbook, Butterworth-Heinemann, 2013.
[33] J.P. Kruth, P. Mercelis, J. Van Vaerenbergh, L. Froyen, M. Rombouts, Binding mechanisms in selective laser sintering and selective laser melting, Rapid prototyping journal, 11(1) (2005) 26-36.
[34] S. Kumar, Selective laser sintering: a qualitative and objective approach, Jom, 55(10) (2003) 43-47.
[35] G.N. Levy, R. Schindel, J.-P. Kruth, Rapid manufacturing and rapid tooling with layer manufacturing (LM) technologies, state of the art and future perspectives, CIRP annals, 52(2) (2003) 589-609.
[36] N. Guo, M.C. Leu, Additive manufacturing: technology, applications and research needs, Frontiers of mechanical engineering, 8(3) (2013) 215-243.
[37] D.T. Pham, R.S. Gault, A comparison of rapid prototyping technologies, International Journal of machine tools and manufacture, 38(10-11) (1998) 1257-1287.
[38] V. Stokes, Thermoplastics as Engineering Materials: The Mechanics, Materials, Design, Processing Link, (1995) 448-455.
[39] I. Zein, D.W. Hutmacher, K.C. Tan, S.H. Teoh, Fused deposition modeling of novel scaffold architectures for tissue engineering applications, Biomaterials, 23(4) (2002) 1169-1185.
[40] M.F. Pietschmann, V. Froehlich, A. Ficklscherer, B. Wegener, V. Jansson, P.E. Müller, Biomechanical testing of a new knotless suture anchor compared with established anchors for rotator cuff repair, Journal of shoulder and elbow surgery, 17(4) (2008) 642-646.

[41] D. Roberson, C.M. Shemelya, E. MacDonald, R. Wicker, Expanding the applicability of FDM-type technologies through materials development, Rapid Prototyping Journal, 21(2) (2015) 137-143.
[42] F.M. Mwema, E.T. Akinlabi, Basics of fused deposition modelling (FDM), in: Fused deposition modeling: strategies for quality enhancement, Springer, 2020, pp. 1-15.
[43] A. Lanzotti, M. Grasso, G. Staiano, M. Martorelli, The impact of process parameters on mechanical properties of parts fabricated in PLA with an open-source 3-D printer, Rapid Prototyping Journal, 21(5) (2015) 604-617.
[44] B.G. Çakan, Effects of raster angle on tensile and surface roughness properties of various FDM filaments, Journal of Mechanical Science and Technology, 35(8) (2021) 3347-3353.
[45] E. Syaefudin, A. Kholil, M. Hakim, D. Wulandari, E. Murtinugraha, The effect of orientation on tensile strength 3D printing with ABS and PLA materials, in: Journal of Physics: Conference Series, IOP Publishing, 2023, pp. 012002.
[46] F. Triawan, D. Syefira, M. Rismalia, I. Suryani, D.W. Djamari, B.A. Budiman, A.B.D. NANDIYANTO, The influence of infill density and pattern on the mechanical and fracture behavior of 3D printed structure subjected to uniaxial tensile load, Journal of Engineering Science and Technology, 17(5) (2022) 3254-3266.
[47] J. Khaliq, D.R. Gurrapu, F. Elfakhri, Effects of Infill Line Multiplier and Patterns on Mechanical Properties of Lightweight and Resilient Hollow Section Products Manufactured Using Fused Filament Fabrication, Polymers, 15(12) (2023) 2585.